molecular pharmaceutics

ARTICLE

pubs.acs.org/molecularpharmaceutics

A Comparison of Spray Drying and Milling in the Production of Amorphous Dispersions of Sulfathiazole/Polyvinylpyrrolidone and Sulfadimidine/Polyvinylpyrrolidone

Vincent Caron, Lidia Tajber, Owen I. Corrigan, and Anne Marie Healy*

School of Pharmacy and Pharmaceutical Sciences, University of Dublin, Trinity College, Dublin 2, Ireland

ABSTRACT: Formulations containing amorphous active pharmaceutical ingredients (APIs) present great potential to overcome problems of limited bioavailability of poorly soluble APIs. In this paper, we directly compare for the first time spray drying and milling as methods to produce amorphous dispersions for two binary systems (poorly soluble API)/excipient: sulfathiazole (STZ)/polyvinylpyrrolidone (PVP) and sulfadimidine (SDM)/PVP. The coprocessed mixtures were characterized by powder X-ray diffraction (PXRD), differential scanning calorimetry (DSC), Fourier transform infrared spectroscopy (FTIR) and intrinsic dissolution tests. PXRD and DSC confirmed that homogeneous glassy solutions (mixture with a single glass transition) of STZ/PVP were obtained for $0.05 \leq X_{PVP}$ (PVP weight fraction) < 1 by spray drying and for $0.6 \leq X_{PVP} < 1$ by milling (at 400 rpm), and homogeneous glassy solutions of SDM/PVP were obtained for $0 < X_{PVP} < 1$ by spray drying and for $0.7 \leq X_{PVP} < 1$ by milling. For these amorphous composites, the value of T_g for a particular API/PVP ratio did not depend on the processing technique used. Variation of T_g versus concentration of PVP was monotonic for all the systems and matched values predicted by the Gordon−Taylor equation indicating that there are no strong interactions between the drugs and PVP. The fact that amorphous SDM can be obtained on spray drying but not amorphous STZ could not be anticipated from the thermodynamic driving force of crystallization, but may be due to the lower molecular mobility of amorphous SDM compared to amorphous STZ. The solubility of the crystalline APIs in PVP was determined and the activities of the two APIs were fitted to the Flory−Huggins model. Comparable values of the Flory−Huggins interaction parameter (χ) were determined for the two systems ($\chi = -1.8$ for SDM, $\chi = -1.5$ for STZ) indicating that the two APIs have similar miscibility with PVP. Zones of stability and instability of the amorphous dispersions as a function of composition and temperature were obtained from the Flory−Huggins theory and the Gordon−Taylor equation and were found to be comparable for the two APIs. Intrinsic dissolution studies in aqueous media revealed that dissolution rates increased in the following order: physical mix of unprocessed materials < physical mix of processed material < coprocessed materials. This last result showed that production of amorphous dispersions by co-milling can significantly enhance the dissolution of poorly soluble drugs to a similar magnitude as co-spray dried systems.

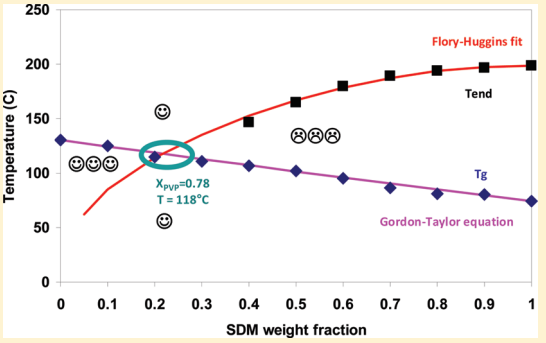

KEYWORDS: glass transition, amorphous dispersion, miscibility, solubility, dissolution, stabilization, spray drying, milling, thermal analysis, DSC, MDSC, X-ray powder diffraction

1. INTRODUCTION

Most current pharmaceutical formulations use the active pharmaceutical ingredients (APIs) in the crystalline state[1] because of their good physical and/or chemical stability if the proper polymorph has been selected during early stages of development.[2] However, an increasing number of newly discovered drugs are classified as II, III or IV in the Biopharmaceutics Classification System (BCS), which means they present a limited bioavailability due to poor solubility and/or poor permeability.[1,3] This represents a hindrance to the emergence of new medicines based on promising therapeutic molecules. Different strategies can be employed to enhance the API solubility, such as cocrystal formation,[4,5] preparation of a salt from of the API[6] or its conversion to an amorphous form.[7,8] The advantage of the latter approach is that it is applicable to any system and does not require chemical modification of the molecule. The amorphous state is a highly disordered, thermodynamically unstable state.[1] The amorphous state has a high Gibbs free energy which results in an improved apparent solubility compared to the crystalline forms and represents a very promising way to overcome bioavailability issues related to poor solubility.[8,9] However, the commercial utilization of amorphous formulations is still marginal because of their unstable nature and the lack of predictive stability.[1,10−12] A parameter of fundamental importance to consider when dealing with the stability of the amorphous state is the glass transition temperature (T_g).[13,14] The T_g represents the crossover between the liquid state, which is disordered with

Received: October 28, 2010
Accepted: February 16, 2011
Revised: January 12, 2011
Published: February 16, 2011

high molecular mobility, and the glassy state, which is disordered with greatly reduced molecular mobility.[12] Therefore, storage at temperatures below the glass transition is required to minimize the likelihood of recrystallization, and the higher the difference between storage temperature and the T_g, the higher the stability of the amorphous phase. As a rule of thumb, it is recommended that glassy pharmaceuticals be stored at least 50 K below T_g[15] since, at this temperature, the molecular mobility (which permits the molecules to rearrange into a crystalline state) is close to zero.[16] For an API which has a T_g close to or below room temperature, storage at a sufficiently low temperature can be a challenge. In order to increase the difference between the T_g of a formulation and storage temperature, preparation of a homogeneous amorphous dispersion of the API with a high-T_g polymeric excipient enables the T_g of the system to be increased compared to the amorphous API.[17−21] The solubility of the API in the polymer[22,23] is also important as it allows the composition at which the amorphous dispersion is saturated with the drug to be identified. Amorphous dispersions with drug contents below or above this composition will be respectively stable or unstable to recrystallization from a thermodynamic point of view. Different methods are available for producing amorphous dispersions, such as melt quenching,[24,25] hot melt extrusion,[8,26] freeze-drying,[27] spray drying[14] or milling.[28−31] Spray drying is an elegant one-step process which allows for the production of particles suitable for inhalation administration, for example.[32−35] The wide variety of processing parameters (choice of solvents, concentration of solutions, feed rate, inlet temperature) makes it a powerful technique to tune the physical state (polymorphic forms, amorphous form) and the particle morphology of pharmaceutical systems.[36] Milling is a solid state process mainly used to reduce particle size in powders. However, it has been shown that the high energy transferred to the powder during milling can also induce changes in the physical state.[29,37,38] Moreover, milling is a solvent-free process and does not induce thermal stresses when correctly designed.[39] These advantages make milling a potential alternative to more commonly used processing techniques (spray drying, freeze drying or melt extrusion for example) where it may not be possible to dissolve the API in a suitable and harmless solvent or when thermal stresses have to be avoided.

The aims of the current study are to compare the ability of milling and spray drying to produce amorphous API/excipient dispersions, to characterize the physicochemical properties of composite systems prepared and to evaluate their dissolution properties in comparison to physical mixtures. The APIs selected were sulfathiazole and sulfadimidine, two poorly soluble antibacterial drugs belonging to the sulfonamides group. Despite their similar molecular structure, these APIs present several differences. Sulfathiazole is a highly polymorphic API with 5 polymorphs discovered so far,[40−42] while sulfadimidine presents only one crystalline form. Moreover, the glass transition temperature of sulfathiazole is more than 20 °C lower than that of sulfadimidine. The excipient used was polyvinylpyrrolidone, an edible polymer soluble in both organic and aqueous solvents. The coprocessed mixtures were characterized by differential scanning calorimetry (standard and modulated), powder X-ray diffraction and infrared spectroscopy to assess the achievement of a homogeneous (i.e., mix at the molecular level) amorphous dispersion as well as interactions between the drugs and the excipient. The solubility of APIs in PVP and Flory−Huggins interaction parameters were determined. Intrinsic dissolution studies were conducted on selected amorphous dispersions and physical mixtures to highlight the advantage of amorphous forms compared to crystalline forms for dissolution of poorly soluble drugs.

2. MATERIALS AND METHODS

2.1. Materials. Sulfathiazole (STZ) (molar weight (M_w) = 255.32 g·mol^{-1}), sulfadimidine (SDM) (M_w = 278.33 g·mol^{-1}) and polyvinylpyrrolidone (PVP) (M_w = 10,000 g·mol^{-1} according to the supplier) were purchased from Sigma-Aldrich and used without further purification. Potassium bromide (KBr) for infrared spectroscopy experiments was purchased from Spectrosol, thoroughly dried before use and stored in a desiccator over silica gel prior to the preparation of KBr disks. Solvents used for the spray drying process were ethanol 99.5% (v/v) (Cooley Distillery, Ireland) and deionized water, prepared using a Millipore Elix 3 RO/EDI system. Buffer solution for dissolution tests was prepared from deionized and vacuum filtered water, potassium dihydrogen phosphate (KH_2PO_4) from BDH Chemicals Ltd. Poole England, and sodium hydroxide (NaOH) from Scharlau Chemie S.A., Spain.

2.2. Methods. *2.2.1. Spray Drying.* The API and excipient were gravimetrically mixed in the required proportions to make 2.5 g of mixtures and dissolved in 500 mL of azeotropic mix of ethanol/water (95.6/4.4 w/w) which has a boiling point of 78.2 °C. The use of an azeotropic mix enables a lower inlet temperature to be used (important to lessen thermal stresses) and to avoid a change in composition of the solvent during the drying step. The obtained solutions were spray dried with a Büchi B-290 mini Spray Dryer (Büchi Laboratoriums-Technik AG, Flawil, Switzerland) operating in the open mode configuration (the drying medium is exhausted to the atmosphere after the spray drying process) with compressed air as the drying gas. In all cases, the spray drying parameters were as follows: air flow of 670 NL·h^{-1}/pump setting of 30% (9 mL·min^{-1}), aspirator setting of 100% (−50 to −60 mbar), inlet temperature of 85 °C, outlet temperature between 56 and 59 °C. The inlet temperature of 85 °C was selected in order to expose the systems to a temperature slightly above the boiling point of the solvent and to ensure good drying of the droplets. A lower inlet temperature would result in incomplete drying, while a higher inlet temperature might result in safety issues and in the systems being exposed to unacceptable thermal stresses. Gel permeation chromatography (GPC) assay was performed, as previously described,[43] on spray dried PVP and confirmed that the molecular weight of PVP was not altered by spray drying.

2.2.2. Milling. Ball milling was performed with a PM 100 high energy planetary mill (Retsch, Germany) at room temperature. Zirconium oxide (ZrO_2) milling jars of 50 cm^3 with 3 balls (∅ = 20 mm) of the same material were used. 2.5 g of API/PVP mixture was placed in the jar corresponding to a ball:sample weight ratio of 32:1. The rotation speed of the solar disk was set to 400 rpm. In order to avoid possible overheating of the container, pause periods of 10 min were made after every 20 min of milling. Total milling time was kept constant at 15 h corresponding to an effective milling time of 10 h. This duration of milling ensured that a stationary state (no more evolution of the physical state of the compounds upon milling[37]) was reached. Milling was performed under normal atmosphere at room temperature. The relative humidity was in the range 25−45% RH during milling. GPC assay[43] was

performed on milled PVP and confirmed that the molecular weight of PVP was not affected by milling.

2.2.3. Melt Quenching. Melt quenching of STZ and SDM was performed by melting the initially crystalline powder, placed in an aluminum weighing boat, on a hot plate (IKA RCT basic, Germany) and quenching the liquid obtained by removing the aluminum weighing boat from the hot plate and allowing to it cool at room temperature. The solid was then gently crushed with a mortar and a pestle. This enabled fully amorphous samples (as determined by powder X-ray diffraction and differential scanning calorimetry) to be prepared.

2.2.4. Powder X-ray Diffraction. Powder X-ray diffraction (PXRD) measurements were performed on samples placed on a low background silicon sample holder (except for co-milled SDM/PVP where a standard glass sample holder was used), using a Rigaku Miniflex II desktop X-ray diffractometer (Rigaku, Tokyo, Japan) with the Bragg−Brentano geometry. The PXRD patterns were recorded from 5° to 40° on the 2θ scale at a step of 0.05°/s. The X-ray tube composed, of Cu anode ($\lambda_{CuK\alpha}$ = 1.54 Å), was operated under a voltage of 30 kV and current of 15 mA.

2.2.5. Thermal Analysis. Differential scanning calorimetry (DSC) experiments were conducted using a Mettler Toledo 821^e with a refrigerated cooling system (LabPlant RP-100). Nitrogen was used as the purge gas. Hermetically sealed 40 μL aluminum pans with three vent holes were used throughout the study, and sample weights varied between 3 and 6 mg. The system was calibrated for temperature and cell constant using indium and zinc. A heating rate of 10 °C/min was implemented in all DSC measurements. Analysis was carried out and monitored by Mettler Toledo STAR^e software (version 6.10) with a Windows NT operating system.

Measurement of heat capacity and relaxation function of amorphous API were obtained using a modulated DSC (MDSC). These experiments were conducted on a DSC Q200 (TA Instruments, United Kingdom) in hermetic pans with 1 pinhole. The instrument was calibrated for temperature and cell constant using high purity indium. Heat capacity readings were calibrated using sapphire. The parameters used for these experiments were as follows: heating rate, 1 °C·min^{-1}; amplitude of modulation, 1 °C; period of modulation, 120 s. The temperature of exothermic or endothermic events given in this paper was the onset temperature. Glass transition temperatures were measured at the midpoint of the C_p shift.

2.2.6. Fourier Transform Infrared Spectroscopy. Infrared spectra were recorded on a Nicolet Magna IT 560 ESP spectrophotometer equipped with MCT/A detector, working under Omnic software version 4.1. A spectral range of 650−4000 cm^{-1}, resolution 2 cm^{-1} and accumulation of 64 scans were used in order to obtain good quality spectra. A potassium bromide (KBr) disk method was used with 0.5% (w/w) sample loading. Disks were prepared by compression under 8 tons for 2 min.

2.2.7. Intrinsic Dissolution Tests. These tests involved dissolution of compressed disks in buffer medium using a paddle over disk method.[45] Disks were prepared by compressing 300 mg of powder in a hydraulic press, for 10 min under 8 tons of pressure, using a 13 mm punch and die set. Powders of physical mixtures were tumbled using a Turbula mixer (Glen Greston Ltd., Middlesex, U.K.) for 30 min at 42 rpm before preparing the disks to ensure good homogeneity.[44] Disks were coated with paraffin wax so that dissolution was possible from one surface only[45] and were affixed to the base of the dissolution vessel using double-sided adhesive tape.

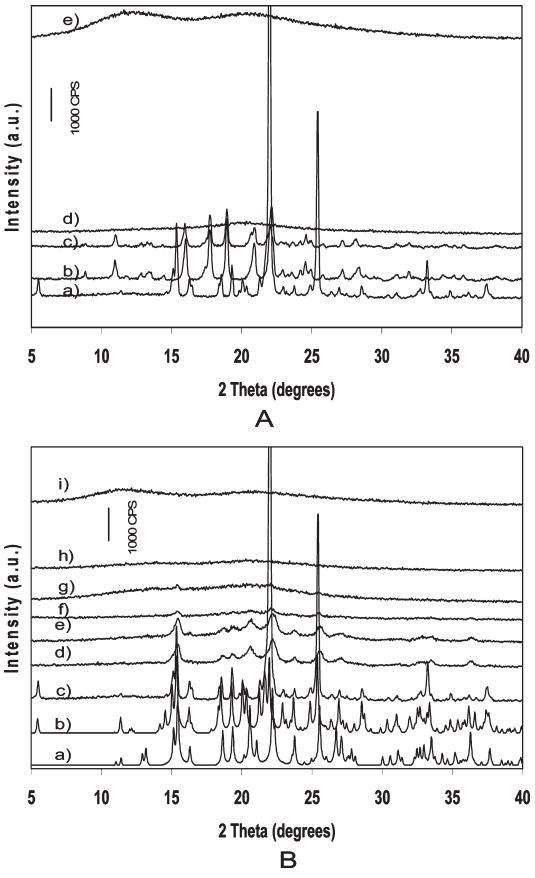

Figure 1. PXRD patterns of coprocessed STZ/PVP mixtures. (A) Co-spray dried mixtures: (a) unprocessed STZ; (b) X_{PVP} = 0; (c) X_{PVP} = 0.02; (d) X_{PVP} = 0.05; (e) X_{PVP} = 1 (X_{PVP} = weight fraction of PVP). (B) Co-milled mixtures: (a) theoretical pattern of STZ IV; (b) theoretical pattern of STZ III; (c) unprocessed STZ; (d) X_{PVP} = 0; (e) X_{PVP} = 0.1; (f) X_{PVP} = 0.3; (g) X_{PVP} = 0.5; (h) X_{PVP} = 0.6; (i) X_{PVP} = 1 (X_{PVP} = weight fraction of PVP).

The dissolution medium used was phosphate buffer solution with pH = 7.0 (250.0 mL of 0.2 M KH_2PO_4 + 145.5 mL of 0.2 M NaOH + 604.5 mL of H_2O) prepared using deionized water.

Dissolution studies were performed using a United States Pharmacopeia paddle apparatus (Erweka DT-6 USP 2). The stirring speed of the paddles was set to 100 rpm, and 900 mL of dissolution medium at 37 ± 0.5 °C was used.

Samples (10 mL) were withdrawn at intervals and filtered through a 0.45 μm membrane filter. The volume removed was replaced with 10 mL of fresh medium at 37 °C. Concentration of the solutions was measured in duplicate by UV spectroscopy.[46] The wavelengths selected were 282 nm for STZ and 263 nm for SDM. "Initial dissolution rates" are dissolution rates determined during the first 5 min of the experiments. "Limiting dissolution rates" are dissolution rates determined between 25 and 30 min of the experiments. A two sample Student's *t*-test ($p \geq 0.95$) was used to determine if dissolution profiles from different experiments were statistically different.

2.2.8. Determination of Solubility of Crystalline APIs in Polymer. The method developed by Tao et al.[23] to determine the solubility of a crystalline API in a polymer was used to determine the solubility of STZ and SDM in PVP. Physical mixtures of API with PVP were prepared by gravimetrically

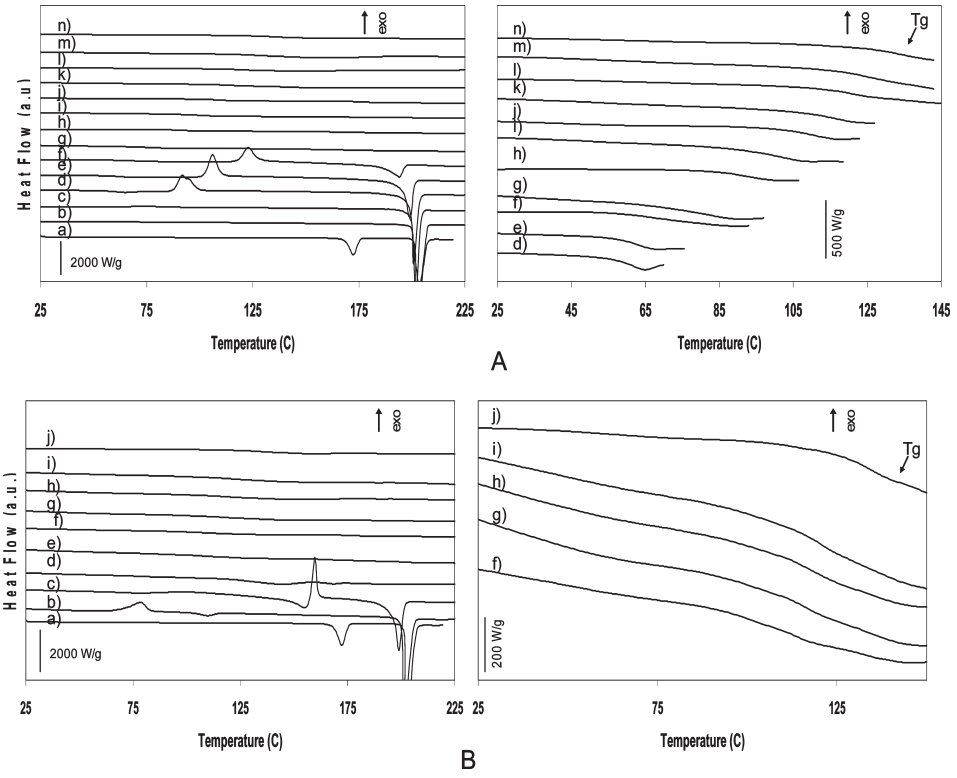

Figure 2. DSC scans of coprocessed STZ/PVP mixtures. Left panels: recrystallization and melting zones. Right panels: glass transition zone. (A) Co-spray dried mixtures: (a) unprocessed STZ; (b) $X_{PVP} = 0$; (c) $X_{PVP} = 0.02$; (d) $X_{PVP} = 0.05$; (e) $X_{PVP} = 0.1$; (f) $X_{PVP} = 0.2$; (g) $X_{PVP} = 0.3$; (h) $X_{PVP} = 0.4$; (i) $X_{PVP} = 0.5$; (j) $X_{PVP} = 0.6$; (k) $X_{PVP} = 0.7$; (l) $X_{PVP} = 0.8$; (m) $X_{PVP} = 0.9$; (n) $X_{PVP} = 1$ (X_{PVP} = weight fraction of PVP). (B) Co-milled mixtures: (a) unprocessed STZ; (b) $X_{PVP} = 0$; (c) $X_{PVP} = 0.1$; (d) $X_{PVP} = 0.3$; (e) $X_{PVP} = 0.5$; (f) $X_{PVP} = 0.6$; (g) $X_{PVP} = 0.7$; (h) $X_{PVP} = 0.8$; (i) $X_{PVP} = 0.9$; (j) $X_{PVP} = 1$ (X_{PVP} = weight fraction of PVP).

mixing the compounds in the required proportions. The mixtures were milled with a mixer mill MM 200 (Retsch, Germany) for 30 min at 70% of maximum intensity of milling in order to improve the uniformity of the physical mix. Care was taken to ensure that crystalline API was still present at the end of milling (checked by PXRD). The mixtures obtained were then held at 100 °C for 5 min in a DSC cell flushed with dry nitrogen to remove moisture, cooled back to room temperature and subjected to a DSC scan at 1 °C·min^{-1} to measure the temperature of the dissolution end point (T_{end}) of the drug in PVP. The relationship between T_{end} and composition allowed the solubility of API in PVP as a function of temperature to be obtained.[23]

3. RESULTS

3.1. Production of Amorphous Composites of STZ/PVP by Coprocessing. *3.1.1. Powder X-ray Diffraction Analysis.* Figure 1 presents the PXRD patterns for co-spray dried (Figure 1A) and co-milled (Figure 1B) STZ/PVP systems. The diffractogram of unprocessed STZ presents sharp and well-defined Bragg peaks, characteristic of the crystalline form III,[47] the stable polymorph at room temperature and atmospheric pressure. The PXRD pattern of PVP is characterized by a diffuse halo with no Bragg peaks, characteristic of an X-ray amorphous material. PXRD patterns of STZ spray dried with X_{PVP} (weight fraction of PVP) < 0.05 show well-defined Bragg peaks characteristic of form I,[47] the polymorph stable at high temperatures. For $X_{PVP} \geq 0.05$, the PXRD patterns do not reveal any peaks and the diffuse halo observed indicates that the systems are X-ray amorphous. Therefore, spray drying resulted in high energy forms (metastable polymorph or unstable amorphous form) of STZ/PVP systems. Compared to previously reported composites of STZ/PVP prepared by coprecipitation,[57] where coprecipitates with $X_{PVP} \leq 0.4$ presented residual crystallinity, the range over which amorphous dispersions can be produced is greatly enhanced with spray drying. This enhancement of the range in which amorphous dispersions can be produced by spray drying compared to coprecipitation has been previously observed[48] for hydroflumethiazide/PVP systems.

Diffractograms of STZ/PVP mixtures ball milled with X_{PVP} < 0.6 revealed residual Bragg peaks which, when compared to the unprocessed API, were broadened and less intense. Broadening of Bragg peaks upon milling has been reported previously for other milled systems and is attributed to a reduction in crystallite size and/or an increase in lattice strain.[49−51] Comparison of the experimental PXRD patterns of milled STZ with those representing the different polymorphs of STZ[47,52−54] indicates that the remaining Bragg peaks can be assigned to form III and/or IV (the theoretical patterns of which are represented in Figure 1B). The broadness of the peaks prevents the clear identification of which of these polymorphs is present or if there is a mixture. For $X_{PVP} \geq 0.6$, the co-milled samples are X-ray amorphous.

3.1.2. Thermal Analysis. Figure 2 presents the DSC scans of co-spray dried (Figure 2A) and co-milled (Figure 2B) STZ/PVP systems. The DSC scan of unprocessed STZ reveals a first endotherm at 168.6 °C due to the transition from form III to form I[40] and a second endotherm at 201.7 °C attributed to the melting of form I. DSC scans of co-spray dried mixtures with

dx.doi.org/10.1021/mp1003674 |*Mol. Pharmaceutics* 2011, 8, 532–542

$0 \leq X_{PVP} \leq 0.02$ present only one thermal event attributed to the melting of form I and are in accordance with the PXRD results (Figure 1A). For $0.05 \leq X_{PVP} \leq 1$, a unique C_p shift characteristic of a glass transition is seen. The T_g shifts from 61 °C for X_{PVP} = 0.05 to 133 °C for X_{PVP} = 1. The presence of a single T_g indicates that the co-spray dried amorphous composites relax as single systems and that the API and the excipient are truly mixed in the amorphous state at the molecular level.[55] Thermal analysis confirms that the diffuse halos seen on PXRD patterns are not the result of nanocrystallinity of the material but are due to a true amorphous state. For $0.05 \leq X_{PVP} \leq 0.3$, an exothermic event occurred at a temperature above the T_g and is attributed to the recrystallization of the amorphous drug phase. PXRD patterns recorded for these mixtures after being heated above the temperature of the exotherms and quenched at room temperature (data not shown) show that the recrystallized form has a PXRD pattern similar to the PXRD of form I. However, an extra peak present at $2\theta = 20.5°$ which does not belong to form I could indicate the presence of a small amount of form III and/or V. The shift of the recrystallization event toward high temperatures as the quantity of PVP increases is consistent with an increased thermal stability of the amorphous mixtures on the time scale of a DSC scan. The shift of the melting event toward lower temperatures with increasing amount of PVP for $0 \leq X_{PVP} \leq 0.3$ is typical of the behavior of a mixture due to the reduction of the chemical potential[56] of the liquid API by the PVP in the liquid mixture. For $X_{PVP} \geq 0.4$, the amorphous composites do not recrystallize during the DSC scan.

DSC scans of co-milled STZ/PVP mixtures for $X_{PVP} \geq 0.6$ reveal a single glass transition, showing that it is also possible to produce amorphous dispersions by co-milling in which the components are mixed at a molecular level. However, a higher quantity of PVP is required to achieve a homogeneous amorphous state compared to co-spray drying. For $X_{PVP} < 0.6$, the thermograms present a complex behavior due to the mixture of amorphous and remaining crystalline form. For example, the DSC scan of the composite with X_{PVP} = 0.5 does not reveal any recrystallization nor melting events although PXRD reveals that crystalline material is still present (Figure 1B). This apparent contradiction was previously observed for other crystalline API/amorphous polymer systems.[8] The explanation for this discrepancy is that, during the DSC scans, the solubility of the API in the polymeric matrix increases as the temperature increases. Therefore, by the time the temperature reaches the melting point of the crystalline drug, it has already been completely dissolved in the polymeric matrix and, consequently, no melting event is recorded.

3.2. Production of Amorphous Composites of SDM/PVP by Coprocessing. *3.2.1. Powder X-ray Diffraction Analysis.* PXRD patterns of SDM/PVP mixtures are displayed in Figure 3A (co-spray dried) and Figure 3B (co-milled). The diffractogram of unprocessed SDM reveals sharp and well-defined Bragg peaks, characteristic of a crystalline material. PXRD patterns of co-spray dried mixtures reveal that the composites are spray dried amorphous for the whole composition range ($0 \leq X_{PVP} \leq 1$).

In contrast, residual peaks seen in the diffractograms of SDM/PVP co-milled mixtures with $X_{PVP} \leq 0.6$ show that SDM remains partly crystalline. For $X_{PVP} \geq 0.7$, a diffuse halo indicates that ball milling produced an amorphous system.

3.2.2. Thermal Analysis. Figure 4A presents the DSC scans of co-spray dried SDM/PVP mixtures. The DSC scan of unprocessed SDM presents one endothermic event at 196.7 °C attributed to the melting of the unique crystalline form of

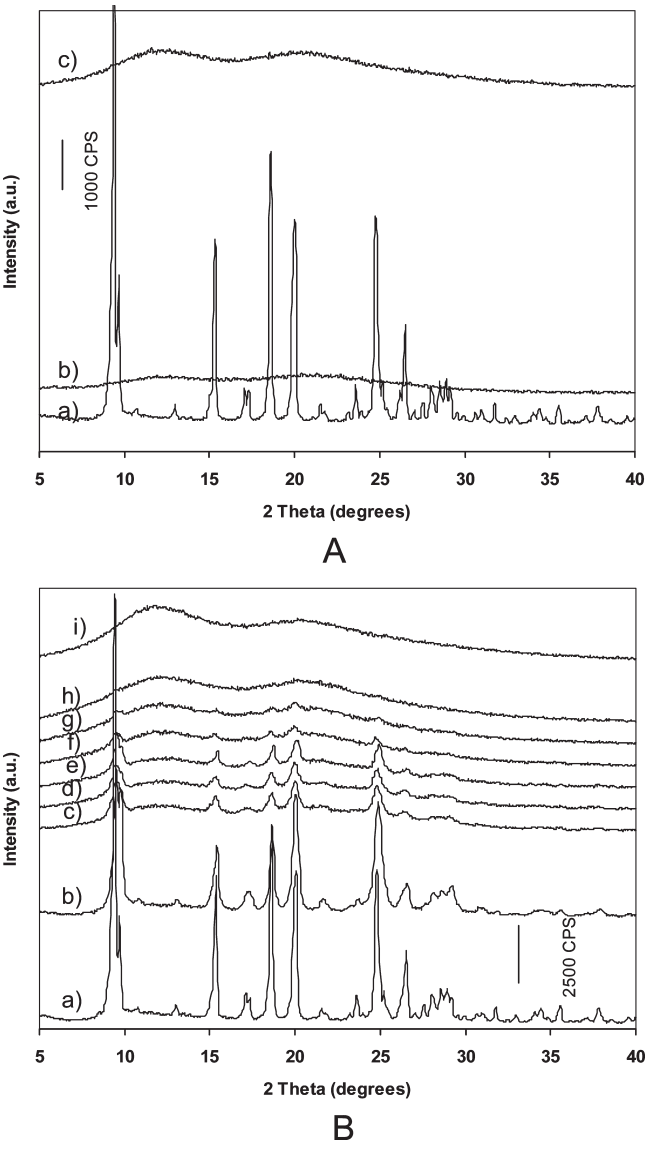

Figure 3. PXRD patterns of coprocessed SDM/PVP mixtures. (A) Co-spray dried mixtures: (a) unprocessed SDM; (b) X_{PVP} = 0; (c) X_{PVP} = 1. (B) Co-milled mixtures: (a) unprocessed SDM; (b) X_{PVP} = 0; (c) X_{PVP} = 0.1; (d) X_{PVP} = 0.2; (e) X_{PVP} = 0.3; (f) X_{PVP} = 0.5; (g) X_{PVP} = 0.6; (h) X_{PVP} = 0.7; (i) X_{PVP} = 1 (X_{PVP} = weight fraction of PVP).

SDM. Co-spray dried mixtures present a single glass transition for $0 \leq X_{PVP} \leq 1$ shifting from 81 °C for X_{PVP} = 0 to 133 °C for X_{PVP} = 1. The T_g of pure spray dried SDM is slightly higher than that determined from quenching the melt in the DSC (74.2 °C ± 0.6). This difference is probably due to the strong endotherm of recovery following the glass transition, observed by DSC for the spray dried sample, which makes an accurate determination difficult. The single T_g present in all the DSC scans of the amorphous mixtures shows that SDM and PVP are homogeneously mixed at a molecular level after spray drying. For $X_{PVP} \leq 0.2$, DSC scans show a recrystallization event followed by melting of the recrystallized SDM. For $X_{PVP} \geq 0.3$, the mixtures do not recrystallize during the DSC analysis.

Figure 4B presents the thermograms of co-milled SDM/PVP mixtures. The only thermal event noticeable for $X_{PVP} \geq 0.7$ is a single glass transition, characteristic of homogeneous amorphous

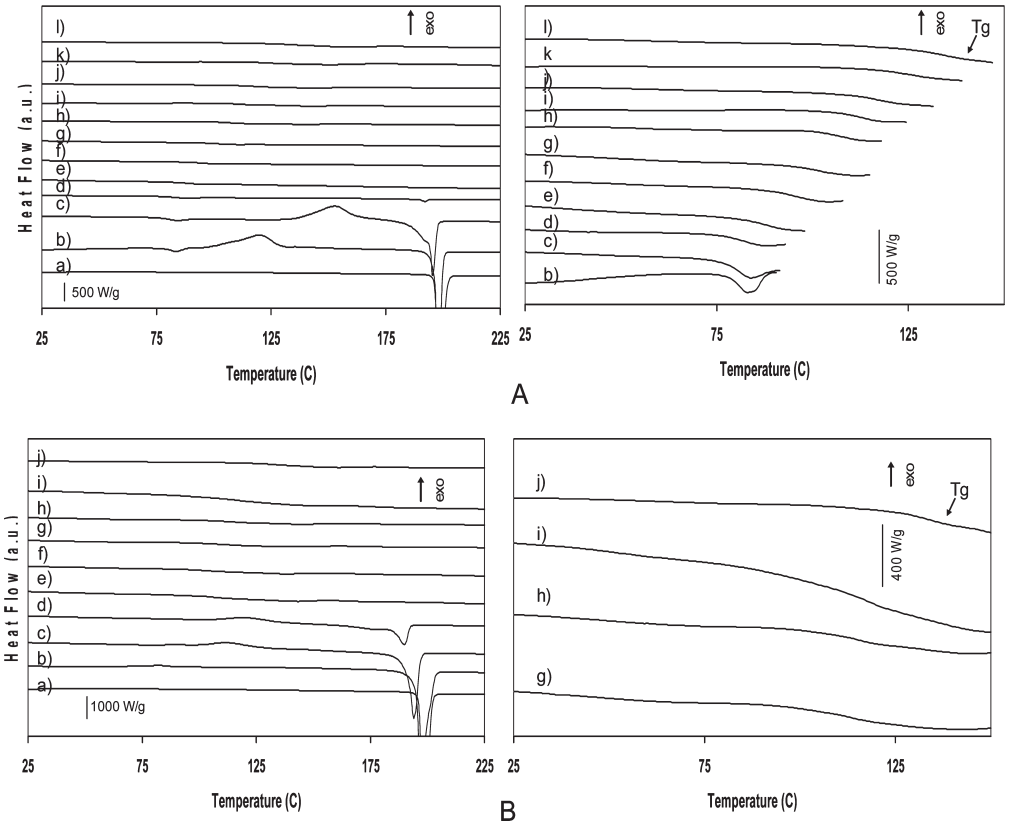

Figure 4. DSC scans of coprocessed SDM/PVP mixtures. Left panels: recrystallization and melting zones. Right panels: glass transition zone. (A) Co-spray dried mixtures: (a) $X_{PVP} = 0$; (b) $X_{PVP} = 0.1$; (c) $X_{PVP} = 0.2$; (d) $X_{PVP} = 0.3$; (e) $X_{PVP} = 0.4$; (f) $X_{PVP} = 0.5$; (g) $X_{PVP} = 0.6$; (h) $X_{PVP} = 0.7$; (i) $X_{PVP} = 0.8$; (j) $X_{PVP} = 0.9$; (k) $X_{PVP} = 1$ (X_{PVP} = weight fraction of PVP). (B) Co-milled mixtures: (a) unprocessed SDM; (b) $X_{PVP} = 0$; (c) $X_{PVP} = 0.1$; (d) $X_{PVP} = 0.2$; (e) $X_{PVP} = 0.5$; (f) $X_{PVP} = 0.6$; (g) $X_{PVP} = 0.7$; (h) $X_{PVP} = 0.8$; (i) $X_{PVP} = 0.9$; (j) $X_{PVP} = 1$ (X_{PVP} = weight fraction of PVP).

Table 1. Dissolution End Points (T_{end}) Measured by DSC for SDM/PVP and STZ/PVP Systems

X_{PVP}[a]	T_{end}(°C) SDM/PVP	T_{end} (°C) STZ/PVP
0.0	198.9 ± 0.1(n = 2)	202.5 ± 0.4 (n = 2)
0.1	196.7 ± 0.0 (n = 2)	199.9 ± 0.3 (n = 2)
0.2	193.8 ± 0.0 (n = 2)	195.4 ± 0.2 (n = 2)
0.3	189.2 ± 0.2 (n = 2)	186.4 ± 1.2 (n = 2)
0.4	179.8 ± 1.5 (n = 2)	173.2 ± 1.7 (n = 2)
0.5	165.1 ± 1.9 (n = 2)	*b*
0.6	146.7 ± 2.8 (n = 2)	*b*

[a] X_{PVP} = weight fraction of PVP. [b] Determination not possible due to the weakness of the thermal events and/or the viscosity of the mixtures. n represents the number of replicates.

dispersions. For $0.3 \leq X_{PVP} \leq 0.6$, although PXRD reveals the presence of crystalline SDM, no thermal events are observed on the thermograms consistent with the dissolution of SDM in PVP during the heating scan. For $0.3 \leq X_{PVP}$, thermograms reveal the presence of a recrystallization event that indicates that SDM was partly amorphized during milling. The recrystallization is then followed by a melting event whose temperature decreases as the proportion of PVP in the mixture increases.

3.3. Solubility of STZ and SDM in PVP. Table 1 presents the relationship between T_{end}, defined as the temperature endset of the melting of the API in the mixture, and weight fraction of API for SDM/PVP and STZ/PVP composites respectively. T_{end} was determined for X_{SDM} (weight fraction of SDM) ≥ 0.4. Below this level, the viscosity of the mixture at T_{end} and the weak intensity of the melting event do not allow the dissolution end point to be accurately determined. In the case of the STZ/PVP systems, the polymorphic transformation III → I for STZ during heating makes the analysis more complicated. For $0.7 \leq X_{STZ} \leq 1$, the DSC scans reveal the presence of a first endotherm between 120 and 160 °C, attributed to the transition of form III toward form I, and a second endotherm at a higher temperature attributed to the melting of form I. The endset of temperature of melting of form I is the one reported as T_{end} because, above this temperature, the only stable form is the liquid (form I is the polymorph with the highest melting point). However, for $X_{STZ} \leq 0.6$, the DSC scans reveal only one endotherm. The nature of this endotherm is not clear. It appears in the temperature range of the transition III → I of STZ, and it is not clear if we see a single endotherm because, for these compositions, the temperature of transition III → I and the temperature of melting of form I overlapped or if, for these compositions, the PVP prevented the conversion of form III toward form I (i.e., for these compositions, form III melts but the resulting liquid cannot recrystallize to form I due to the presence of PVP). In order to circumvent this problem, we produced STZ form I by spray drying and used it to make physical mixtures STZ/PVP for $X_{STZ} \leq 0.6$. This allowed T_{end} for $X_{STZ} = 0.6$ to be determined. For $X_{STZ} \leq 0.5$, the high viscosity of the mixture at T_{end} and the weak intensity of the melting do not allow an accurate determination of the dissolution end points.

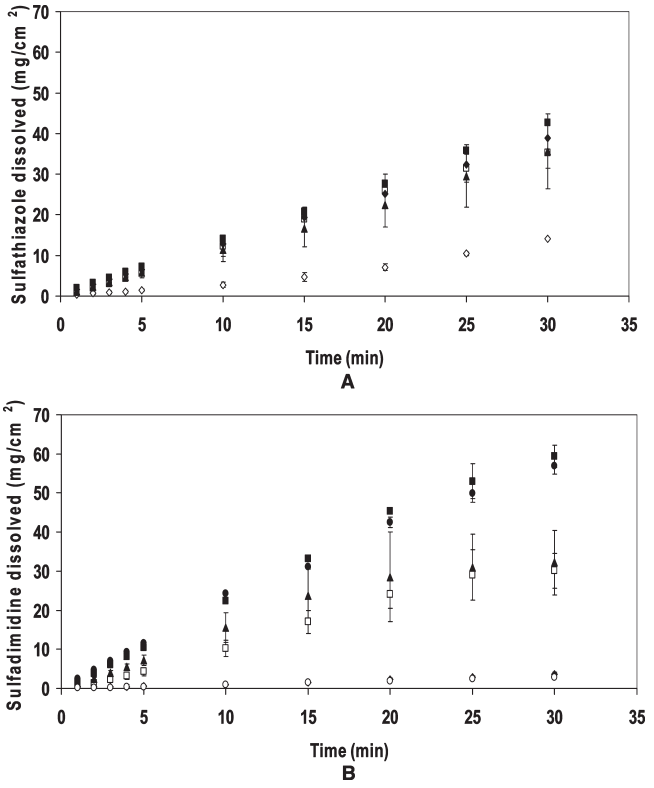

Figure 5. Intrinsic dissolution profiles for different mixtures of API/PVP with weight fraction of PVP (X_{PVP}) = 0.7: (A) STZ/PVP mixtures; (B) SDM/PVP mixtures. Open circles: pure unprocessed API. Diamonds: physical mixtures of unprocessed API and unprocessed PVP. Open squares: physical mixtures of API and PVP milled separately. Triangle: physical mixtures of API and PVP spray dried separately. Solid squares: API and PVP co-milled. Solid circles: API and PVP co-spray dried.

3.4. Dissolution Tests. Figure 5 presents intrinsic dissolutions profiles of STZ/PVP mixtures (Figure 5A) and SDM/PVP (Figure 5B) with X_{PVP} = 0.7. This composition is chosen because, for this level of PVP, homogeneous amorphous dispersions are produced by spray drying or by milling for the two APIs. Five different mixtures of API with PVP are considered for each of the two systems: the physical mixture of unprocessed materials, the physical mixture of materials milled separately, the physical mixture of materials spray dried separately, the co-milled system and the co-spray dried system. Figure 5B presents also the dissolution profile of pure unprocessed SDM. It is not possible to perform this test on pure STZ as the compressed disks crumbled before the test could start. As SDM spray dried alone is amorphous, the physical mixture of SDM/PVP spray dried separately is a purely amorphous system. PXRD patterns recorded on the material remaining at the end of the dissolution test for the physical mixtures of SDM/PVP spray dried separately show Bragg peaks (data not shown) and may explain the curvature seen on the dissolution curve of these samples. On the other hand, amorphous dispersions obtained by coprocessing are sufficiently physically stable to remain amorphous during the dissolution tests. For the two API/PVP systems, the dissolution profile of co-milled mixtures is found not to be statistically different from the dissolution profile of the co-spray dried samples. Dissolution rates and dissolution rate enhancements of processed mixtures compared to mixtures of unprocessed materials are reported in Table 2. This table shows that, for the two API/PVP systems studied, dissolution rates increase in the following order: physical mix of unprocessed materials < physical mix of processed material < coprocessed materials. This result shows that production, by either technique, of amorphous dispersions enhances the dissolution rate of poorly soluble drugs. Dissolution rate enhancements in SDM/PVP systems are much higher than is observed for STZ/PVP systems. It is noteworthy that the relative enhancement in initial dissolution rates for STZ/PVP are comparable to the values observed by Simonelli et al.[57] for coprecipitates. These authors suggested on the basis of solubility data the formation of a complex between STZ and PVP which contributed to the dissolution enhancement. The greater increase in dissolution rates of SDM/PVP compared to STZ/PVP could be due to the formation of a more soluble complex for the former system.

4. DISCUSSION

4.1. Driving Force for Crystallization and Molecular Mobility of Amorphous SDM and Amorphous STZ. The first step of spray drying consists of making a solution of the pharmaceutical systems with a suitable solvent. This means that, before spray drying, the systems are in a liquid state and are disordered. However, after spray drying, SDM is amorphous while STZ is crystallized as form I, the metastable form at room temperature.

DSC scans were undertaken of amorphous SDM and amorphous STZ prepared by melt quenching (as it is not possible to obtain amorphous STZ by spray drying or milling). The onset of crystallization of amorphous STZ (101 °C) was found to be nearly 30 °C lower than the onset of crystallization of amorphous sulfadimidine (129 °C), indicating that amorphous STZ is less thermally stable than amorphous SDM.

The amorphous state and the prediction of the final state (i.e., amorphous, crystalline) upon processing are still topics which are poorly understood. However, several tools are mentioned in the literature that facilitate an understanding of why some states are preferably obtained upon processing. Both the thermodynamic driving force for crystallization and molecular mobility are frequently invoked as valuable tools in understanding stability problems associated with recrystallization of the amorphous phase.[10,11,58,59] The driving force for crystallization, which is the difference in free energy of a system in supercooled liquid and crystalline state, was estimated using the Hoffman approach[60] (eq 1):

$$\Delta G_C = \Delta H_m \frac{(T_m - T)T}{T_m^2} \quad (1)$$

ΔG_C represents the difference in free energy of the API in the supercooled liquid state and in the crystalline state, ΔH_m and T_m represent the enthalpy and temperature of melting respectively, and T is the temperature at which ΔG_C is calculated. Figure 6 presents the driving force for crystallization versus temperature for SDM and STZ. According to this figure, SDM presents a greater driving force for crystallization than STZ from 0 up to 185 °C. Therefore, amorphous SDM should be less stable than amorphous STZ from a thermodynamic point of view. Therefore, as the experimental data do not agree with the prediction that can be made from the thermodynamic driving force for crystallization, it can be ruled out as the main factor accounting for the differences observed between spray dried sulfathiazole and sulfadimidine.

Table 2. Intrinsic Dissolution Rates (DR) and Enhancement in Dissolution Rates Compared to Physical Mixtures of Unprocessed Materials for STZ/PVP and SDM/PVP Systems

	dissolution rate ($mg \cdot min^{-1} \cdot cm^{-2}$)							
	initial				limiting			
	STZ/PVP		SDM/PVP		STZ/PVP		SDM/PVP	
	DR[a]	DR enhancement[b]	DR[a]	DR enhancement[b]	DR[a]	DR enhancement[b]	DR[a]	DR enhancement[b]
physical mix of unprocessed materials	0.27	1	0.08	1	0.75	1	0.15	1
physical mix of materials milled separately	1.11	4.11	0.85	10.63	0.76	1.01	0.22	1.46
physical mix of materials spray dried separately	1.15	4.26	1.45	18.13	1.22	1.63	0.24	1.60
co-milled materials	1.41	5.22	2.12	26.50	1.31	1.75	1.28	8.53
co-spray dried materials	1.29	4.78	2.30	28.75	1.35	1.80	1.37	9.13

[a] DR is the dissolution rate (determined as the slope of the dissolution curves represented in Figure 5). [b] DR enhancement is the ratio of the dissolution rate of the sample under consideration and the dissolution rate of the physical mixture of unprocessed API/PVP system.

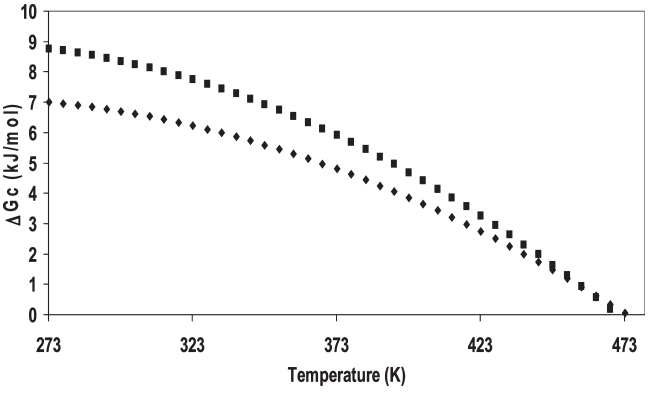

Figure 6. Driving force for crystallization versus temperature for amorphous STZ (diamonds) and amorphous SDM (squares) determined from eq 1.

The relaxation function (which is a measure of the molecular mobility of an amorphous system below T_g) is obtained by determining the enthalpy of recovery at the glass transition of an amorphous system aged at the temperature of interest (annealed) for increasing periods of time.[61] The experimental relaxation is given by eq 2:[10]

$$\phi(t,T) = 1 - \frac{\Delta H(t,T)}{\Delta H(\infty,T)} \quad (2)$$

where $\Delta H(t,T)$ is the enthalpy of recovery (J/g) determined by integrating the area, obtained during a MDSC scan, under the nonreversing signal obtained for an annealed sample. The contributions to annealing due to relaxation during the heating ramp and the frequency effect were eliminated by subtracting the area under the nonreversing signal of a nonannealed sample ($t = 0$). $\Delta H(\infty,T)$ is the maximal enthalpy recovery of a sample which is determined by eq 3:[10]

$$\Delta H(\infty,T) = \Delta C_p(T_g - T) \quad (3)$$

The relaxation parameter is equal to 1 for a nonrelaxed system and reaches 0 for a fully relaxed system. Figure 7 presents the relaxation function versus aging time at 39 °C for SDM and STZ. It shows that, at a given temperature below T_g, SDM relaxes more slowly than STZ thus the molecular mobility of amorphous STZ

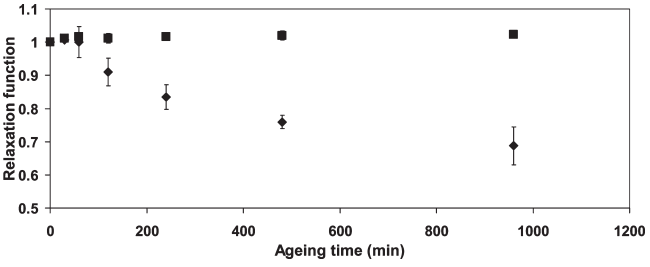

Figure 7. Relaxation function determined at 39 °C for amorphous STZ (diamonds) and amorphous SDM (squares).

is therefore greater than the molecular mobility of amorphous SDM at this temperature. The greater molecular mobility of amorphous STZ compared to amorphous SDM is consistent with the fact that the T_g of SDM is higher than the T_g of STZ. Consequently, at a given temperature, amorphous SDM is more supercooled than amorphous STZ. Therefore, the greater ability of STZ to recrystallize compared to SDM during the spray drying process may be controlled by the kinetics of the amorphous state.

Changing spray drying conditions to spray dry the two sulfonamides with the same degree of supercooling with respect to their T_g, i.e. with the same ($T_{outlet} - T_g$), in order to test further the molecular mobility origin of the different behavior of SDM and STZ upon spray drying, would not be conclusive, as doing so would change other parameters (drying rate of droplets in the drying chamber, driving force for crystallization, residual humidity of the spray dried powders) that could influence the physical stability of the spray dried samples.

4.2. Homogeneity of Amorphous Dispersions and Determination of the Zones of Physical Stability and Instability on a Composition−Temperature Diagram for SDM/PVP and STZ/PVP Amorphous Dispersions. The activity of a substance in a mixture can be obtained from eq 4:[22]

$$\ln a = \frac{\Delta H_m}{R} \times \left(\frac{1}{T_m} - \frac{1}{T_{end}}\right) \quad (4)$$

where a is the activity, ΔH_m is the enthalpy of melting ($J \cdot mol^{-1}$) of the pure API, R is the gas constant ($J.K^{-1} \cdot mol^{-1}$), T_m is the melting point (K) of the pure API, and T_{end} (K) is the temperature at which the drug's solubility is measured. Figure 8 represents the activity of the crystalline APIs in PVP as a function of PVP weight fraction.

dx.doi.org/10.1021/mp1003674 |*Mol. Pharmaceutics* 2011, 8, 532–542

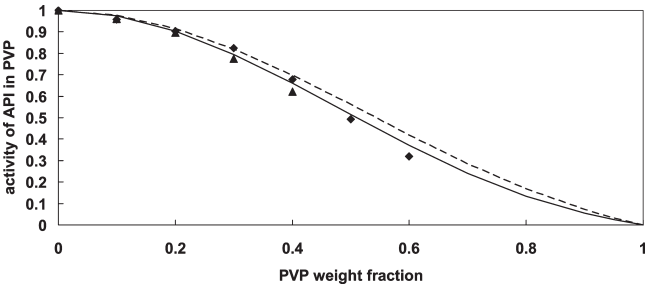

Figure 8. Activity of API in PVP versus PVP weight fraction. Triangles and dashed line represent respectively the experimental activity and the fit of the experimental data with the eq 5 for STZ/PVP systems (χ = −1.5; R^2 = 0.99). Diamond and solid line represent respectively the experimental activity and the fit of the experimental data with the eq 5 for SDM/PVP systems (χ = −1.8; R^2 = 0.99).

With regard to STZ/PVP systems, the activity is determined for $0.6 \leq X_{STZ} \leq 1$ as T_{end} for lower PVP concentrations is uncertain. According to the Flory−Huggins model, the activity of an API in a polymer can be described by eq 5:[22]

$$\ln a = \ln v_1 + \left(1 - \frac{1}{x}\right) v_2 + \chi {v_2}^2 \qquad (5)$$

where v_1 is the volume fraction of API, v_2 is the volume fraction of polymer, x is the molar volume ratio of PVP and API, and χ is the Flory−Huggins (FH) interaction parameter. The lines in Figure 8 represent the fit of the experimental activities by eq 5. For the two systems under consideration, the FH model accurately describes the experimental relationship between activity and polymer weight fraction. For STZ and SDM, interaction parameters of −1.5 and −1.8 respectively were obtained by fitting. These negative values indicate that the APIs and PVP are miscible. Moreover, the fact that the FH interaction parameters are comparable for the two APIs means that they have similar miscibility with PVP.

Figure 9A and Figure 9B present the experimental solubilities of the APIs in PVP, the solubilities in PVP calculated from the FH model, the experimental relationship between T_g and weight fraction of API and the relationship between T_g and weight fraction of API predicted by the Gordon−Taylor law with Simha−Boyer rule.[62,63] Table 3 gives all the parameters necessary to determine the calculated solubilities from eqs 4 and 5 and the predicted changes in T_g from the Gordon−Taylor law.

The changes of T_g with PVP concentration are similar whether the amorphous dispersions are produced by spray drying or by milling and are monotonic for all the systems under investigation. The fact that the changes in T_g with composition are well predicted by the Gordon−Taylor law reveals that there are no strong interactions[31] between the APIs and the PVP in the amorphous dispersions. FTIR spectra (data not shown) of these mixtures do not reveal shifts in the IR bands of the compounds involved in hydrogen bonds and confirm the absence of significant interactions.

According to Tao et al.,[23] the quantity $(T_{end} - T_g)$ for a given composition defines how close the dissolution end point of the API in the polymer is to the glass transition. These data enable the composition at which the binary mixtures form a saturated solution at the glass transition, i.e. the composition where $(T_{end} - T_g)$ is equal to zero, to be determined. This particular composition is X_{PVP} = 0.78 at 118 °C for SDM in PVP and

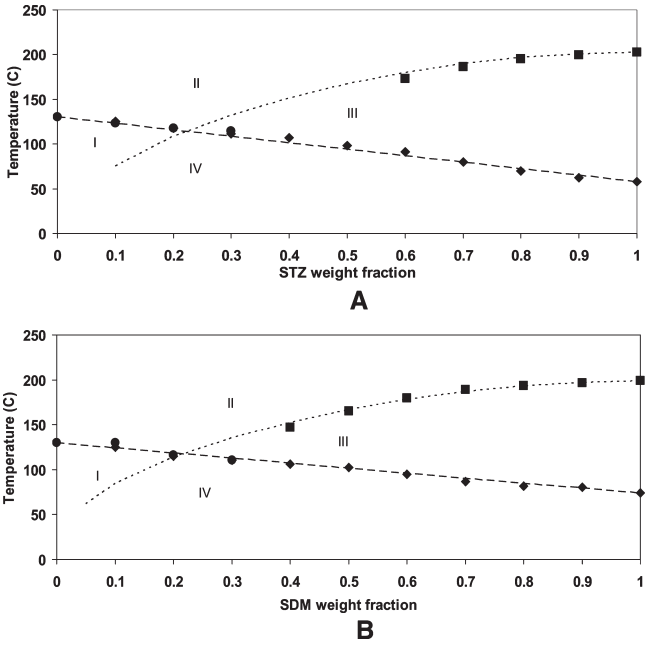

Figure 9. T_{end} (dissolution end point) and T_g (glass transition temperature) as a function of API concentration. Diamonds represent experimental T_g from spray dried dispersions, circles represent experimental T_g from milled dispersions, squares represent experimental T_{end}, dashed line represents the Gordon−Taylor law, and dotted line represents T_{end} calculated from eqs 4 and 5: (A) STZ/PVP systems; (B) SDM/PVP mixtures.

X_{PVP} = 0.78 at 114 °C for STZ in PVP. This is an important parameter in terms of design of physically stable amorphous dispersions because from this data, four temperature−composition regions (named I, II, III and IV in Figure 9) can be defined. Region I is a region where the solution of the API in PVP is undersaturated and below the T_g, making it physically stable from a thermodynamic point of view and in which the molecular mobility is low, therefore reducing the likelihood of chemical degradation (not investigated in this article). Region II is a region where the solution of the API in PVP is undersaturated and above the T_g, making it physically stable from a thermodynamic point of view but in which the high molecular mobility might lead to chemical degradations. Region III is a region where the solution of the API in PVP is supersaturated and above the T_g, making it unstable from a thermodynamic point of view and in which the high molecular mobility might lead both to physical instability and to chemical degradation. Region IV is a region where the solution of the API in PVP is supersaturated and below the T_g, making it unstable from a thermodynamic point of view but in which the low molecular mobility might reduce the likelihood of crystallization and chemical degradation.

Preliminary studies of physical stability of the amorphous systems prepared by either milling or spray drying show that all remain X-ray amorphous after more than 1 year of storage at 4 °C with desiccant, with the exception of pure sulfadimidine spray dried and the STZ/PVP dispersion with X_{PVP} = 0.05 prepared by spray drying for which, in both cases, PXRD patterns reveal the presence of Bragg peaks.

4.3. Production of Amorphous Dispersions by Spray Drying or by Milling. At least for the systems under consideration in this study, spray drying allows amorphous dispersions of API/PVP to be produced over a wider concentration range than

Table 3. Thermal Characteristics of STZ, SDM and PVP

compds/properties	T_m (K)	ΔH_m (kJ·mol^{-1})	T_g (K)	density (g·cm^{-3})	ΔC_p (J·K^{-1}·g^{-1})
sulfathiazole	473.8 ± 0.1 (n = 3)	28.7 ± 0.2 (n = 3)	331.1 ± 0.8 (n = 7)	1.53 (extrapolation from density of amorphous composites)	0.44 ± 0.02 (n = 3)
sulfadimidine	470.6 ± 0.1 (n = 3)	36.0 ± 0.3 (n = 3)	347.3 ± 0.6 (n = 7)	1.34 ± 0.00 (n = 5)	0.51 ± 0.01 (n = 3)
PVP	*b*	*b*	403.4 ± 5.1 (n = 3)	1.23 ± 0.00 (n = 5)	0.22[a]

[a] Reference 14. [b] Not relevant (PVP is an amorphous polymer and therefore does not present melting events). n represents the number of replicates.

milling. The two techniques are very different in nature so it is not straightforward to establish why spray drying permits the concentration range over which an amorphous dispersion is obtained to be expanded compared to milling. However, several points can be made. The reason for the better efficiency of spray drying in obtaining amorphous systems compared to milling is certainly due to the fact that spray drying involves a rapid drying of a solution, which is by nature a disordered system in which the two compounds (API and excipient) are already molecularly dispersed. Therefore, obtaining an amorphous system by this process would mainly require "only" evaporating the solvent quickly enough to prevent nucleation and/or growth of crystalline materials. On the other hand, milling involves comminution of a crystalline API with PVP and therefore a first step before mixing the two components at a molecular level requires breaking the crystalline lattice of the API. This may be the reason why it is unable to produce amorphous systems for high concentrations of API. Moreover, achievement of amorphous dispersions by a particular processing technique depends on the processing parameters related to this technique. So changing these parameters might enable the concentration range over which amorphous dispersions are obtained to be changed. For spray drying, numerous parameters can be tuned, such as composition of the solution, concentration, feed rate and inlet temperature. Parameters for ball milling are powder/ball mass ratio, hardness of the material of the grinding container, milling time, rotation speed (which is linked to the intensity of milling), temperature of milling and relative humidity at which milling is performed. According to Descamps and co-workers, other important parameters concerning the amorphization of materials upon milling are the relative position of the glass transition temperature of the milled systems compared to the milling temperature[28,29,37,64] and the relative humidity during milling.[37] The lower the temperature of milling and the lower the relative humidity, the better the chances of producing an amorphous sytem by milling.

5. CONCLUSION

In this paper, we have, for the first time, made a direct comparison of spray drying and milling as processes which can be used to produce amorphous dispersions. Spray drying allowed amorphous dispersions to be obtained over a wider concentration range than milling for the systems under investigation.

Flory−Huggins interaction parameters and Gordon−Taylor plots allowed the boundaries of the zones of stability and instability of the amorphous dispersions of STZ/PVP and SDM/PVP on a temperature−composition plot to be defined. The composition at which the binary mixtures formed a saturated solution at the glass transition was determined to be the same for the two systems in spite of the differing glass transition temperatures of the two APIs.

The fact that SDM could be spray dried amorphous but not STZ (spray dried as a metastable polymorph) despite molecular similarities between the two APIs could not be anticipated from the thermodynamic driving forces of crystallization but rather seemed to have a kinetic origin

Both co-spray dried and co-milled amorphous dispersions showed better dissolution rates in aqueous solution compared to physical mixtures of unprocessed materials and physical mixtures of materials processed separately. Improvement of dissolution rate is a significant challenge with poorly soluble drugs and the result obtained here showed that production of amorphous dispersions can result in significantly increased drug dissolution rates.

Preliminary stability studies showed that all the amorphous dispersions remained amorphous upon storage at 4 °C with desiccant after more than one year except SDM spray dried alone and the STZ/PVP dispersion with X_{PVP} = 0.05 prepared by spray drying that present partial crystallinity. Further stability studies will be conducted and included in future work.

AUTHOR INFORMATION

Corresponding Author

*University of Dublin, Trinity College, School of Pharmacy and Pharmaceutical Sciences, Panoz Institute, Dublin 2, Ireland. E-mail: healyam@tcd.ie. Tel: +353 (0) 1 896 1444.

ACKNOWLEDGMENT

This paper is based upon works supported by the Science Foundation Ireland under Grant No. [07/SRC/B1158] as part of the Solid State Pharmaceutical Cluster (SSPC).

REFERENCES

(1) Bhugra, C.; Pikal, M. J. *J. Pharm. Sci.* **2008**, *97* (4), 1329–1349.
(2) Singhal, D.; Curatolo, W. *Adv. Drug Delivery Rev.* **2004**, *56* (3), 335–347.
(3) Moore, M. D.; Wildfong, P. L. D. *J. Pharm. Innovation* **2009**, *4* (1), 36–49.
(4) Stanton, M. K.; Tufekeic, S.; Morgan, C.; Bak, A. *Cryst. Growth Des.* **2009**, *9* (3), 1344–1352.
(5) Good, D. J.; Rodrıguez-Hornedo, N. *Cryst. Growth Des.* **2009**, *9* (5), 2252–2264.
(6) Huang, L. F.; Tong, W. Q. *Adv. Drug Delivery Rev.* **2004**, *56* (3), 321–334.
(7) Forster, A.; Hempenstall, J.; Rades, T. *J. Pharm. Pharmacol.* **2001**, *53* (3), 303–315.
(8) Patterson, J. E.; James, M. B.; Forster, A. H.; Lancaster, R. W.; Butler, J. M.; Rades, T. *Int. J. Pharm.* **2007**, *336* (1), 22–34.
(9) Murdande, S. B.; Pikal, M. J.; Shanker, R. M.; Bogner, R. H. *J. Pharm. Sci.* **2010**, *99* (3), 1254–1264.
(10) Bhugra, C.; Shmeis, R.; Krill, S.; Pikal, M. J. *Pharm. Res.* **2006**, *23* (10), 2277–2290.
(11) Bhugra, C.; Shmeis, R.; Krill, S. L.; Pikal, M. J. *J. Pharm. Sci.* **2008**, *97* (1), 455–472.
(12) Bhattacharya, S.; Suryanarayanan, R. *J. Pharm. Sci.* **2009**, *98* (9), 2935–2953.

(13) Craig, D. Q. M.; Royall, P. G.; Kett, V. L.; Hopton, M. L. *Int. J. Pharm.* **1999**, *179* (2), 179–207.
(14) Tajber, L.; Corrigan, O. I.; Healy, A. M. *Eur. J. Pharm. Sci.* **2005**, *24* (5), 553–563.
(15) Hancock, B. C.; Shamblin, S. L.; Zografi, G. *Pharm. Res.* **1995**, *12* (6), 799–806.
(16) Hancock, B. C.; Shamblin, S. L. *Thermochim. Acta* **2001**, *380* (2), 95–107.
(17) Marsac, P. J.; Shamblin, S. L.; Taylor, L. S. *Pharm. Res.* **2006**, *23* (10), 2417–2426.
(18) Khougaz, K.; Clas, S. D. *J. Pharm. Sci.* **2000**, *89* (10), 1325–1334.
(19) Crowley, K. J.; Zografi, G. *Pharm. Res.* **2003**, *20* (9), 1417–1422.
(20) Taylor, L. S.; Zografi, G. *Pharm. Res.* **1997**, *14* (12), 1691–1698.
(21) Leuner, C.; Dressman, J. *Eur. J. Pharm. Biopharm.* **2000**, *50* (1), 47–60.
(22) Sun, Y.; Tao, J.; Zhang, G. G. Z.; Yu, L. *J. Pharm. Sci.* **2010**, *99* (9), 4023–4031.
(23) Tao, J.; Sun, Y.; Zhang, G. G. Z.; Yu, L. *Pharm. Res.* **2009**, *26* (4), 855–864.
(24) Shmeis, R. A.; Wang, Z.; Krill, S. L. *Pharm. Res.* **2004**, *21* (11), 2025–2030.
(25) Yu, L. *Adv. Drug Delivery Rev.* **2001**, *48* (1), 27–42.
(26) Forster, A.; Hempenstall, J.; Tucker, I.; Rades, T. *Int. J. Pharm.* **2001**, *226* (1−2), 147–161.
(27) Lu, X.; Pikal, M. J. *Pharm. Dev. Technol.* **2004**, *9* (1), 85–95.
(28) Caron, V.; Willart, J. F.; Danede, F.; Descamps, M. *Solid State Commun.* **2007**, *144* (7−8), 288–292.
(29) Descamps, M.; Willart, J. F.; Dudognon, E.; Caron, V. *J. Pharm. Sci.* **2007**, *96* (5), 1398–1407.
(30) Dudognon, E.; Willart, J. F.; Caron, V.; Capet, F.; Larsson, T.; Descamps, M. *Solid State Commun.* **2006**, *138* (2), 68–71.
(31) Willart, J. F.; Descamps, N.; Caron, V.; Capet, F.; Danède, F.; Descamps, M. *Solid State Commun.* **2006**, *138* (4), 194–199.
(32) Tajber, L.; Corrigan, D. O.; Corrigan, O. I.; Healy, A. M. *Int. J. Pharm.* **2009**, *367* (1−2), 79–85.
(33) Chow, A. H. L.; Tong, H. H. Y.; Chattopadhyay, P.; Shekunov, B. Y. *Pharm. Res.* **2007**, *24* (3), 411–437.
(34) Shoyele, S. A.; Cawthorne, S. *Adv. Drug Delivery Rev.* **2006**, *58* (9−10), 1009–1029.
(35) Vehring, R. *Pharm. Res.* **2008**, *25* (5), 999–1022.
(36) Tajber, L.; Corrigan, O. I.; Healy, A. M. *Int. J. Pharm.* **2009**, *367* (1−2), 86–96.
(37) Willart, J. F.; Descamps, M. *Mol. Pharmaceutics* **2008**, *5* (6), 905–920.
(38) De Gusseme, A.; Neves, C.; Willart, J. F.; Rameau, A.; Descamps, M. *J. Pharm. Sci.* **2008**, *97* (11), 5000–5012.
(39) Willart, J. F.; Caron, V.; Lefort, R.; Danede, F.; Prevost, D.; Descamps, M. *Solid State Commun.* **2004**, *132* (10), 693–696.
(40) Zeitler, J. A.; Newnham, D. A.; Taday, P. F.; Threlfall, T. L.; Lancaster, R. W.; Berg, R. W.; Strachan, C. J.; Pepper, M.; Gordon, K. C.; Rades, T. *J. Pharm. Sci.* **2006**, *95* (11), 2486–2498.
(41) Kelleher, J. M.; Lawrence, S. E.; Moynihan, H. A. *CrystEngComm* **2006**, *8* (4), 327–332.
(42) Apperley, D. C.; Fletton, R. A.; Harris, R. K.; Lancaster, R. W.; Tavener, S.; Threlfall, T. L. *J. Pharm. Sci.* **1999**, *88* (12), 1275–1280.
(43) Tewes, F.; Tajber, L.; Corrigan, O. I.; Ehrardt, C.; Healy, A. M. *Eur. J. Pharm. Sci.* **2010**, *41* (2), 337–352.
(44) Nolan, L. M.; Tajber, L.; McDonald, B. F.; Barham, A. S.; Corrigan, O. I.; Healy, A. M. *Eur. J. Pharm. Sci.* **2009**, *37* (5), 593–602.
(45) Corrigan, O. I.; Timoney, R. F. *J. Pharm. Pharmacol.* **1975**, *27* (10), 759–764.
(46) Healy, A. M.; Corrigan, O. I. *Int. J. Pharm.* **1992**, *84* (2), 167–173.
(47) Kruger, G. J.; Gafner, G. *Acta Crystallogr., B* **1972**, *28*, 272–283.
(48) Corrigan, O. I.; Holohan, E. M. *J. Pharm. Pharmacol.* **1984**, *36* (4), 217–221.
(49) Langford, J. I.; Louer, D. *Rep. Prog. Phys.* **1996**, *59* (2), 131–234.
(50) Louer, D. *Acta Crystallogr., Sect. A: Found. Crystallogr.* **1998**, *54* (6), 922–933.
(51) Willart, J. F.; Lefebvre, J.; Danede, F.; Comini, S.; Looten, P.; Descamps, M. *Solid State Commun.* **2005**, *135* (8), 519–524.
(52) Kruger, G. J.; Gafner, G. *Acta Crystallogr., B* **1971**, *27*, 326–333.
(53) Hughes, D. S.; Hursthouse, M. B.; Threlfall, T.; Tavener, S. *Acta Crystallogr., C* **1999**, *55*, 1831–1833.
(54) Babilev, F. V.; Bel'skii, V. K.; Simonov, Y. A.; Arzamastsev, A. P. *Khim.-Farm. Zh.* **1987**, *21*, 1275–1280.
(55) Timko, R. J.; Lordi, N. G. *Drug Dev. Ind. Pharm.* **1984**, *10* (3), 425–451.
(56) Atkins, P.; De Paula, J. *Physical Chemistry for the Life Sciences*; Oxford University Press: 2006; p 135.
(57) Simonelli, A. P.; Mehta, S. C.; Higuchi, W. I. *J. Pharm. Sci.* **1969**, *58* (5), 538–549.
(58) Caron, V.; Bhugra, C.; Pikal, M. *J. Pharm. Sci.* **2010**, *99* (9), 3887–3900.
(59) Gupta, P.; Chawla, G.; Bansal, A. K. *Mol. Pharmaceutics* **2004**, *1* (6), 406–413.
(60) Rumondor, A. C. F.; Marsac, P. J.; Stanford, L. A.; Taylor, L. S. *Mol. Pharmaceutics* **2009**, *6* (5), 1492–1505.
(61) Hancock, B. C.; Zografi, G. *J. Pharm. Sci.* **1997**, *86* (1), 1–12.
(62) Gordon, M.; Taylor, J. S. *J. Appl. Chem.* **1952**, *2*, 493–500.
(63) Simha, R.; Boyer, R. F. *J. Chem. Phys.* **1962**, *37* (5), 1003–1007.
(64) Dujardin, N.; Willart, J. F.; Dudognon, E.; Hedoux, A.; Guinet, Y.; Paccou, L.; Chazallon, B.; Descamps, M. *Solid State Commun.* **2008**, *148* (1−2), 78–82.